ELSEVIER

Journal of Quantitative Spectroscopy & Radiative Transfer 109 (2008) 2417–2426

Journal of Quantitative Spectroscopy & Radiative Transfer

www.elsevier.com/locate/jqsrt

Photoionization cross sections of Fe XXI

Sultana N. Nahar*

Department of Astronomy, The Ohio State University, 140 W. 18th Ave., Columbus, OH 43210, USA

Received 28 November 2007; received in revised form 11 March 2008; accepted 22 March 2008

Abstract

Total and partial photoionization cross sections for (Fe XXI + $h\nu \rightarrow$ Fe XXII + e) are presented for the ground and excited bound states with $n \leqslant 10$ and $l \leqslant 9$. Fe XXI is prevalent in high-temperature astrophysical plasmas as well as in photoionized plasmas excited by hard X-rays. Results are reported for the first time for the high-energy photoionization with core excitations to $n = 2, 3$ states. Details of photoionization, especially the high-energy features that often dominate considerably over the low energy ones, are illustrated. These prominent features will affect the photoionization and the recombination rates in high-temperature plasmas. Calculations are carried out in the close coupling (CC) approximation using the R-matrix method. A large CC wavefunction expansion for Fe XXII which includes the ground and 28 excited core states from $n = 2$ and 3 complexes and spans over a wide energy range is used. A total of 835 discrete bound states of Fe XXI in the singlet, triplet, and quintet symmetries are obtained. Total photoionization cross sections, $\sigma_{\rm PI}(nLS)$, for ionization into all 29 states are presented for all 835 final bound states and partial photoionization cross sections, $\sigma_{\rm PI}(g, nLS)$, for ionization into the ground $^2P^0$ state of the core are presented for 685 states. While the $n = 2$ core excitations are at relatively lower energy range (within 15 Ry from the ionization threshold), the $n = 3$ excitations lie at considerably higher energy, 73 Ry and above, yet introduce resonant features and enhancements more prominent than those of $n = 2$ states. Larger numbers of resonances are formed due to Rydberg series of autoionizing states converging on to the 29 core states. However, most noticeable structures are formed in the excited state cross sections by the photoexcitation-of-core (PEC) resonances in the photon energy range of 73–82 Ry. All these high-energy features are absent in the currently available results. The present results should enable more accurate modeling of the emission spectrum of highly excited plasma from the optical to far-ultraviolet region.

PACS: 31.15.vj; 32.80.Fb; 32.80.Zb

Keywords: Photoionization; Fe XXI; High-energy features; Effect on solar opacity

1. Introduction

Fe XXI exists in high-temperature plasmas in various astronomical objects, such as in nebulae, active galactic nuclei, stars, solar flares, etc. The 1354 Å line of Fe XXI which forms at temperature of 10^7 K is well known for coronal diagnostics (e.g. [1]). Astrophysical modelings for opacities, spectral analysis, ionization

*Corresponding author. Tel: +1 614 292 1888; fax: +1 614 292 2928.
E-mail address: nahar@astronomy.ohio-state.edu

0022-4073/$ - see front matter © 2008 Published by Elsevier Ltd.
doi:10.1016/j.jqsrt.2008.03.008

balance, recombination cascade matrix, etc., require photoionization cross sections, such as presented here, from a large number of initial bound states (e.g. [2,3]).

Previous works on Fe XXI under the Opacity Project [4] were mainly for total photoionization cross sections from a large number of bound states. However, since these calculations were designed to cover only the low energy region [5,6] they considered a smaller wavefunction expansion containing only eight core states of $n = 2$ complex. The same set, but with fine structure, was used by Zhang [7] to calculate photoionization cross sections from the three fine structure levels of the ground state. In contrast to the earlier works, the present work considers a larger wavefunction which reveals a number of new and important high-energy features. In addition, the present work reports for the first time the partial photoionization cross sections from 685 states needed for various applications such as for recombination rates.

Also being reported here, for non-fine structure modeling needs, is a large set of oscillator strengths in *LS* coupling for transitions among all 835 LS terms computed using the bound state wavefunctions and dipole matrix elements of the present work. They are consistent with the present photoionization cross sections. These are available in electronic files at [8]. The oscillator strengths for fine structure transitions calculated from the relativistic Breit–Pauli R-matrix method were reported earlier [9].

2. Theory

The present calculations are carried out in the close coupling (CC) approximation using the R-matrix method as implemented in the work under the Opacity Project (OP) [4] and the Iron Project (IP) [10]. A brief outline of the theory relevant to the present calculations is given below. The details of the R-matrix method in the CC approximation are given in [11–14].

In the CC approximation, the 'target' or the 'core' ion is represented by an N-electron system interacting with the $(N + 1)$th electron. The $(N + 1)$th electron may be bound or in the continuum depending on its negative or positive energy (E). The total wavefunction, Ψ_E, of the $(N + 1)$ electrons system in a symmetry $SL\pi$ is represented by an expansion as

$$\Psi_E(e + ion) = A \sum_i \chi_i(ion)\theta_i + \sum_j c_j \Phi_j, \tag{1}$$

where the target ion eigenfunction, χ_i, is coupled with the $(N + 1)$th electron function, θ_i. The sum is over the ground and excited core states. The $(N + 1)$th electron with kinetic energy k_i^2 is in a channel labeled as $S_i L_i \pi_i k_i^2 \ell_i (SL\pi)$. In the second sum, the Φ_j's are bound channel functions of the $(N + 1)$-electron system that account for short range correlation and the orthogonality between the continuum and the bound electron orbitals.

The Hamiltonian of the $(N + 1)$-electrons system is given by

$$H_{N+1}^{\mathrm{BP}} = \sum_{i=1}^{N+1} \left\{ -\nabla_i^2 - \frac{2Z}{r_i} + \sum_{j>i}^{N+1} \frac{2}{r_{ij}} \right\} + H_{N+1}^{\mathrm{mass}} + H_{N+1}^{\mathrm{Dar}} + H_{N+1}^{\mathrm{so}}, \tag{2}$$

where the last three terms are relativistic corrections, the mass correction (H^{mass}), Darwin (H^{Dar}) and spin–orbit interaction (H^{so}), respectively (e.g. [20]). Present calculations are carried out in LS coupling, that is, no spin–orbit interaction is considered. However, contributions from relativistic corrections H^{mass} and H^{Dar} are included. Substitution of $\Psi_E(e + ion)$ in the Schrodinger equation

$$H_{N+1}\Psi_E = E\Psi_E \tag{3}$$

introduces a set of coupled equations that are solved using the R-matrix approach. The solution is a continuun wavefunction, Ψ_F, for an electron with positive energies ($E > 0$), or a bound state, Ψ_B, at a *negative* total energy ($E \leqslant 0$). The complex resonant structures in photoionization result from channel couplings between continuum channels that are open ($k_i^2 > 0$), and ones that are closed ($k_i^2 < 0$), at electron energies k_i^2 corresponding to autoionizing states of the Rydberg series, $S_i L_i \pi_i \nu\ell$ where ν is the effective quantum number, converging to the target thresholds.

Transition matrix elements for photoionization, $\langle \Psi_B \| \mathbf{D} \| \Psi_F \rangle$ where $\mathbf{D} = \sum_i r_i$ is the dipole operator and the sum is over the number of electrons, are obtained from the bound and continuum wavefunctions. For bound–bound transitions, Ψ_F is replaced by another bound state. The transition matrix element can be reduced to generalized line strength as

$$\mathbf{S} = |\langle \Psi_j \| \mathbf{D}_L \| \Psi_\mathrm{i} \rangle|^2 = \left| \left\langle \psi_\mathrm{f} \left| \sum_{j=1}^{N+1} r_j \right| \psi_\mathrm{i} \right\rangle \right|^2, \tag{4}$$

where Ψ_i and Ψ_f are the initial and final state wavefunctions. The photoionization cross section (σ_PI) is proportional to the generalized line strength as

$$\sigma_\mathrm{PI} = \frac{4\pi^2}{3c} \frac{1}{g_i} \omega \mathbf{S}, \tag{5}$$

where g is the statistical weight factor of the bound state and ω is the incident photon energy. The oscillator strengths can be obtained from

$$f_{ij} = \frac{E_{ij}}{3g_i} S(i,j).$$

3. Computations

Computation for photoionization cross sections of Fe XXI is carried out using the R-matrix suite of codes from the OP and IP [13–15] that proceeds through a number of stages. The initial stage is to obtain through atomic structure calculations the target or core wavefunction which forms the first term of the ion wavefunction Ψ_E. The target orbitals are the input for stage 1 of R-matrix codes.

The present wavefunction for Fe XXI includes 29 target terms of Fe XXII, eight from $n = 2$ and 21 from $n = 3$ complexes as given in Table 1. The table lists the energies used in the R-matrix calculations. For accurate energy positions of the resonances the calculated target (Fe XXII) energies were replaced by the observed energies, whenever available [16], during diagonalization of the $(N + 1)$-electron Hamiltonian. The

Table 1
Terms and energies of Fe XXII in the eigenfunction expansion of Fe XXI

	Term	E (Ry)		Term	E (Ry)
$n = 2$ *states*			15	$2s2p3p(^4S)$	78.08464*
1	$2s^2 2p(^2P^0_{1/2})$	0.0	16	$2s2p3p(^4P)$	78.38718*
2	$2s2p^2(^4P^e)$	4.350891	17	$2s2p3p(^2P)$	78.85499
3	$2s2p^2(^2D^e)$	6.837967	18	$2s2p3p(^2S)$	79.09630*
4	$2s2p^2(^2S^e)$	8.620770	19	$2s2p3s(^2P^0)$	79.41596*
5	$2s2p^2(^2P^e)$	8.914198	20	$2s2p3p(^2D)$	80.21885
6	$2p^3(^4S^0)$	11.442782	21	$2s2p3d(^2P^0)$	80.53455*
7	$2p^3(^2D^0)$	12.891660	22	$2s2p3d(^4F^0)$	80.77472
8	$2p^3(^2P^0)$	14.656426	23	$2s2p3p(^2P)$	80.90579*
$n = 3$ *states*			24	$2s2p3p(^2D)$	80.97771*
9	$2s^2 3s(^2S)$	73.24894*	25	$2s2p3d(^4P^0)$	81.31389
10	$2s^2 3p(^2P^0)$	74.83334*	26	$2s2p3p(^2S)$	81.39861*
11	$2s2p3s(^4P^0)$	76.37739*	27	$2s2p3d(^2D^0)$	81.44906
12	$2s2p3s(^2P^0)$	77.20010*	28	$2s2p3d(^4D^0)$	81.48460
13	$2s^2 3d(^2D)$	77.48869	29	$2s2p3d(^2F^0)$	82.45406
14	$2s2p3p(^4D)$	77.81568			

A large energy gap (~60 Ry) can be noticed between $n = 2$ and 3 states. The asterisks indicate calculated energies since the measured values are not available.

observed term energies were obtained from the statistical average of the observed fine structure levels and are scaled relative to the actual ground level of Fe XXII which is $2s^2 2p(^2P^0_{1/2})$. The reason for choosing the ground level $^2P^0_{1/2}$, instead of the ground term $^2P^0$, is that all fine structure levels are relative to the $^2P^0_{1/2}$. An asterisk next to an energy in the column indicates use of the calculated energy, that is, no measured value is available for the state. The atomic structure calculation for the target Fe XXII included spectroscopic configurations $2s^22p$, $2s2p^2$, $2p^3$, $2s^23s$, $2s^23p$, $2s^23d$, $2s2p3s$, $2s2p3p$, $2s2p3d$ and correlation configurations $2s3d^2$, $2p^23s$, $2p^23p$, $2p^23d$. The wavefunction for Fe XXII was obtained from atomic structure calculations using the code SUPERSTRUCTURE [17] which employs Thomas–Fermi–Dirac potential to generate the one-electron orbitals. The target was optimized with various sets of configurations. The calculated higher energies are in better agreement with the observed term energies than are the lower energies. Hence, the final set was chosen that showed the best overall agreement with measured values.

The second sum in the wavefunction expansion, Eq. (1), includes all possible $(N+1)$-electron configurations with range of minimum and maximum occupancies listed within parentheses of the orbitals as $2s(0-2)$, $2p(0-4)$, $3s(0-2)$, $3p(0-2)$, and $3d(0-2)$ of Fe XXI. All $SL\pi$ symmetries of the $(e+ion)$ system formed from the 29 target states coupled with an interacting electron with partial waves $0 \leqslant l \leqslant 9$ are included.

Due to large memory and CPU time requirements, the computation on Cray machines was carried out separately for singlets, triplets, and quintets and in four energy ranges. Total and partial photoionization cross sections are computed independently as R-matrix codes employ different storage algorithms for them.

All bound state energies of Fe XXI were identified using quantum defect analysis and percentage channel contributions to the states. The near threshold resonances of $\sigma_{\rm PI}$ were resolved in a finer energy mesh, with 4000 energies up to 0.4 Ry above the ionization threshold. $\sigma_{\rm PI}$ at higher photoelectron energies, beyond the highest target threshold, are extrapolated as in [18] and were processed by the code ELEVID [19].

4. Results and discussions

Results from detailed study of photoionization of the highly charged iron ion, Fe XXI, are presented. The work emphasizes on high-energy photoionization cross sections that show dominant features for the ion obtained for the first time.

An explanation is needed for the choice of the size of the wavefunction. For any ion, the high lying excited core states do not form bound states and the effects of their correlations with lower energy channels are usually weak. Hence, for practical computation, a wavefunction expansion is limited to an excited core state when a large energy gap is found with the higher ones. For the Fe XXI core, the eight $n=2$ states are relatively close and lie within 14.5 Ry, but $n=3$ states start after a large energy gap of about 60 Ry. Hence, the electron–electron correlation effects from $n=3$ terms are expected to be negligible, and this was the reason for them to be excluded in the previous calculations for photoionization cross sections [5,6]. These existing cross sections show smooth decay in the high-energy region. It has turned out that the B-like core Fe XXII is found to be an exception to the correlation effects. It was noticed from atomic structure calculations that the radiative decay rates (A-values) for $n=3$ terms are a few orders of magnitude higher than those of $n=2$ terms [21] providing the incentive to study the effect of strong dipole transitions in the core in the high-energy region.

4.1. Bound energy states of Fe XXI

A total of 835 bound states of Fe XXI are found with $n \leqslant 10$ and $0 \leqslant l \leqslant 9$. Of these only 27 states have been observed (e.g. compilation by NIST [16]). These states have the core either in the ground and in one of seven excited states of $n=2$ complex (Table 1). No bound state with excited $n=3$ core states are formed for Fe XXI. The complete set of 835 energies with spectroscopic designation will be available electronically [8].

The observed and calculated energies of Fe XXI are compared in Table 2. The agreement is good in general. However, discrepancies are found for some excited states as seen in the table, with the largest one being 6.8% for $2s22p5d(^1F^0)$ state. There could be a few reasons for the differences. Although a large number of configurations were considered in the calculations, the set still may not be large enough for higher accuracy.

Table 2
Comparison of calculated energies, E_c, of Fe XXI with the measured values, E_0 [16]

Conf.	Term	E_0 (Ry)	E_c (Ry)
$2s22p2$	^3P	123.30	124.09
$2s22p2$	^1D	121.89	123.11
$2s22p2$	^1S	120.73	121.99
$2s2p3$	$^5S^0$	119.68	120.55
$2s2p3$	$^3D^0$	116.92	117.72
$2s2p3$	$^3P^0$	115.61	116.71
$2s2p3$	$^3S^0$	114.13	114.88
$2s2p3$	$^1D^0$	113.85	114.89
$2s2p3$	$^1P^0$	112.62	113.87
$2p4$	^3P	108.74	109.48
$2p4$	^1D	107.56	108.57
$2p4$	^1S	105.45	106.65
$2s22p3d$	$^1D^0$	50.32	50.65
$2p3d$	$^3F^{0*}$	50.29	50.63
$2s22p3d$	$^3D^{0*}$	49.46	50.21
$2s22p3d$	$^3P^{0*}$	49.11	50.14
$2s22p3d$	$^1P^0$	48.54	49.53
$2s22p3d$	$^1F^0$	48.36	49.48
$2s22p4d$	$^3F^{0*}$	27.94	28.16
$2s22p4d$	$^3P^{0*}$	27.33	27.99
$2s22p4d$	$^3D^0$	27.01	28.02
$2s22p4d$	$^1D^0$	26.84	28.16
$2s22p4d$	$^1F^0$	26.78	27.76
$2s22p5d$	$^3D^0$	16.57	17.27
$2s22p5d$	$^3P^0$	16.49	15.96
$2s22p5d$	$^1D^0$	16.49	17.16
$2s22p5d$	$^1F^0$	16.46	17.59

The target may have needed better optimization. The present *LS* coupling approximation includes only two relativistic corrections terms. Energies should have improved with more relativistic corrections.

As mentioned earlier, the calculated states were identified spectroscopically through quantum defect analysis. However, identification of all states cannot be ascertained because of mixed states and having similarities in quantum defects. For example, a series of Rydberg states can be singled out from quantum defect and increment of effective quantum numbers by unity. However, for an ion with large number of bound states, such as Fe XXI, some uncertainty is introduced since two or more *nl* series can have very similar effective quantum numbers. Also in the computation, the order of two core states $2s2p^2(^2S,^2P)$ (Table 1) was reversed to the observed order and hence some shifting is assumed in excited states with these two core excitations.

4.2. Total and partial photoionization cross sections of Fe XXI

The *total* photoionization cross sections $\sigma_{\rm PI}(nLS)$, which include contributions from all channels leaving the ion in all 29 core states are presented for all 835 bound states of Fe XXI. The *partial* photoionization cross sections, for ionization into the ground $2s^22p(^2P^0)$ state of the residual ion Fe XXII, are obtained for all 684 states of the singlets and the triplets that couple to the target ground state. Quintets do not couple to the core ground state in *LS* coupling. Since partial photoionization does not include contributions of ionization with an excited core, $\sigma_{\rm PI}(g, nLS)$ has a background that is lower than that of the total and lacks the corresponding resonances. Some important characteristic features of these cross sections are illustrated below.

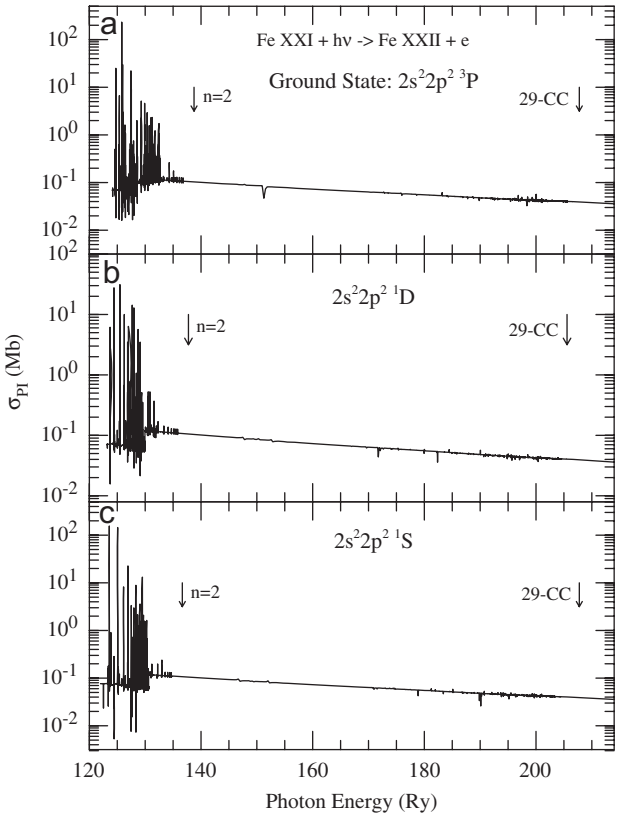

Fig. 1. Photoionization cross sections, $\sigma_{\rm PI}$, of the three states of the ground configuration, $1s^2 2s^2 2p^2$ of Fe XXI: (a) the ground state, ^3P, (b) excited state ^1D, and (c) excited state, ^1S. The prominent resonances in the low energy region are due to autoionizing states of the Rydberg series belonging to the eight core states of the $n = 2$ complex and the sparsely distributed weak resonances in the high energy belong to the $n = 3$ complex. The highest thresholds of the $n = 2$ and 3 (29-CC) complexes are designated by arrows.

Fig. 1 presents the total $\sigma_{\rm PI}$ for the three states $^3P,^1D,^1S$ of the ground configuration $1s^2 2s^2 2p^2$ of Fe XXI. Each state shows significant resonances in the near threshold energy region extending over to the eight core states of $n = 2$ complex. These resonances will affect both photoionization and recombination rates in the low energy and low temperature regions. The highly excited $n = 3$ core states in the 29-CC expansion do not affect $\sigma_{\rm PI}$ except introducing some very weak small resonances on the smooth background. Comparison of the present cross sections is made with those from the Opacity Project in Fig. 2. The two states, ground state and metastable state $2s2p^3(^3D^0)$, are selected where the high-energy background show some differences with and without $n = 3$ core excitations. However, the present resolution in cross sections is much finer than that in the OP and should be more accurate.

The structure of the photoionization cross section at high energies changes considerably for excited valence electron states when the effect of the $n = 3$ excited states of the core is included. This is illustrated in Fig. 3. The figure presents total photoionization cross sections of two excited states of Fe XXI: $2s^2 2p 3d(^3D^0)$ (a—present 29-CC calculations, b—from the OP) and $2s^2 2p 3p(^3D)$ (c—present 29-CC calculations, d—from the OP). Comparison between the present $\sigma_{\rm PI}$ with those from the OP [5] shows gross underestimation by the latter. The first resonant complex in the low energy region, appearing less prominent in the figure, belongs to Rydberg series of autoionizing states of $n = 2$ core states. Rest of the features, which are more extensive and stronger than the $n = 2$ ones, spanning over a large energy range are due to $n = 3$ core states. These resonances have enhanced the background considerably. Larger radiative decay rates of $n = 3$ states have caused these strong resonances. Important effects of $n = 3$ core states of other carbon-like ions were noted earlier [18]. However, such prominent effects were not unexpected for Fe XXI because of large energy gaps between $n = 2$

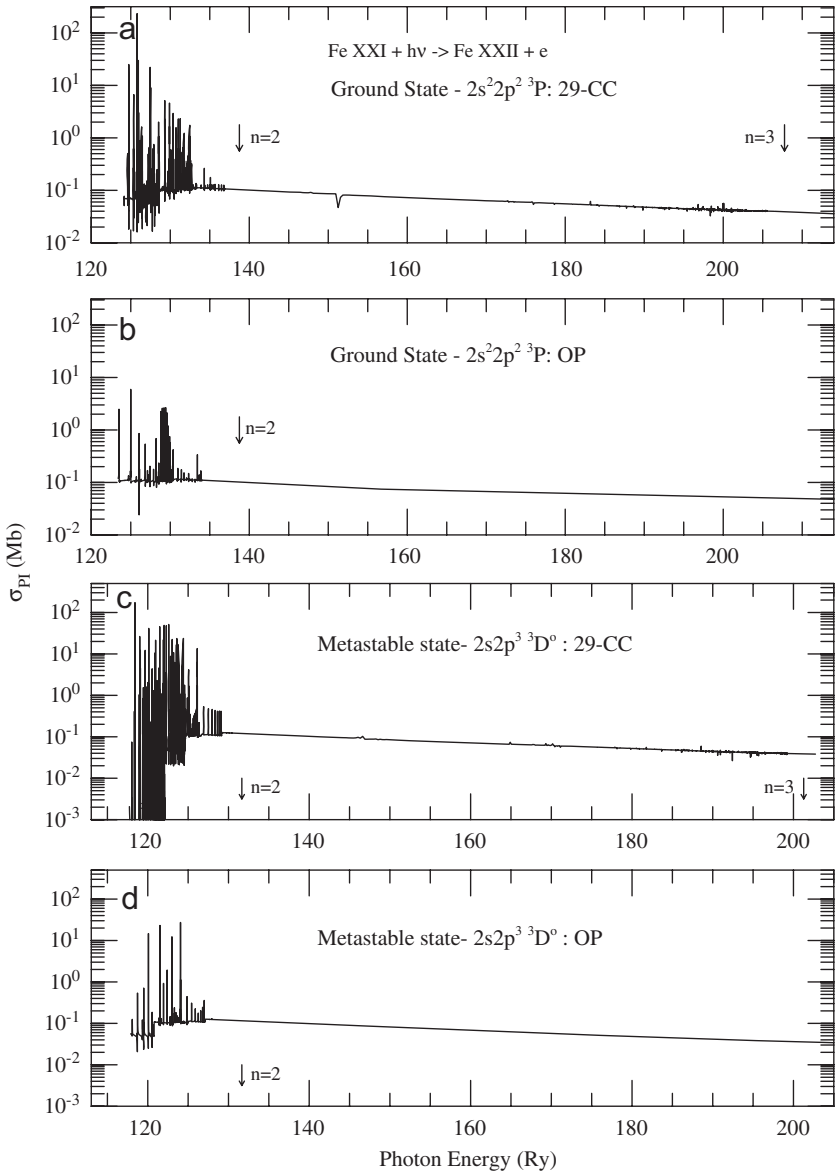

Fig. 2. Comparison of present photoionization cross sections, σ_{PI}, from 29-CC calculations with those from the OP [5]: (a,b) ground state ^3P, (c,d) metastable state $2s2p^3(^3D^0)$. Present σ_{PI} is much more highly resolved than those given by the Opacity Project.

and 3 complexes. The present features indicate that the correlations of channels with excited $n = 3$ core states contribute considerably to photoionization contradicting the earlier assumption of weaker couplings.

The resonances due to $n = 3$ core states can be divided into two types: narrow Rydberg resonances and broader photoexcitation-of-core (PEC) resonances. The enhanced resonant complex region in the photon energy range of 73–82 Ry noted in Figs. 3(a,c) is due mainly to the PEC resonances. PEC resonances were first explained and named by Seaton in [22]. They are the important characteristic features of valence electron excited states. A PEC resonance is formed when the ion absorbs a photon in a dipole allowed core excitation from the ground state. During this process the outer electron remains temporarily attached to a highly excited level and autoionizes as the core drops to the ground state. This process is inverse to dielectronic recombination and is manifested in a large resonance at the excitation threshold energy. A PEC resonance is wider than the narrow Rydberg resonances and can enhance the background cross section by orders of

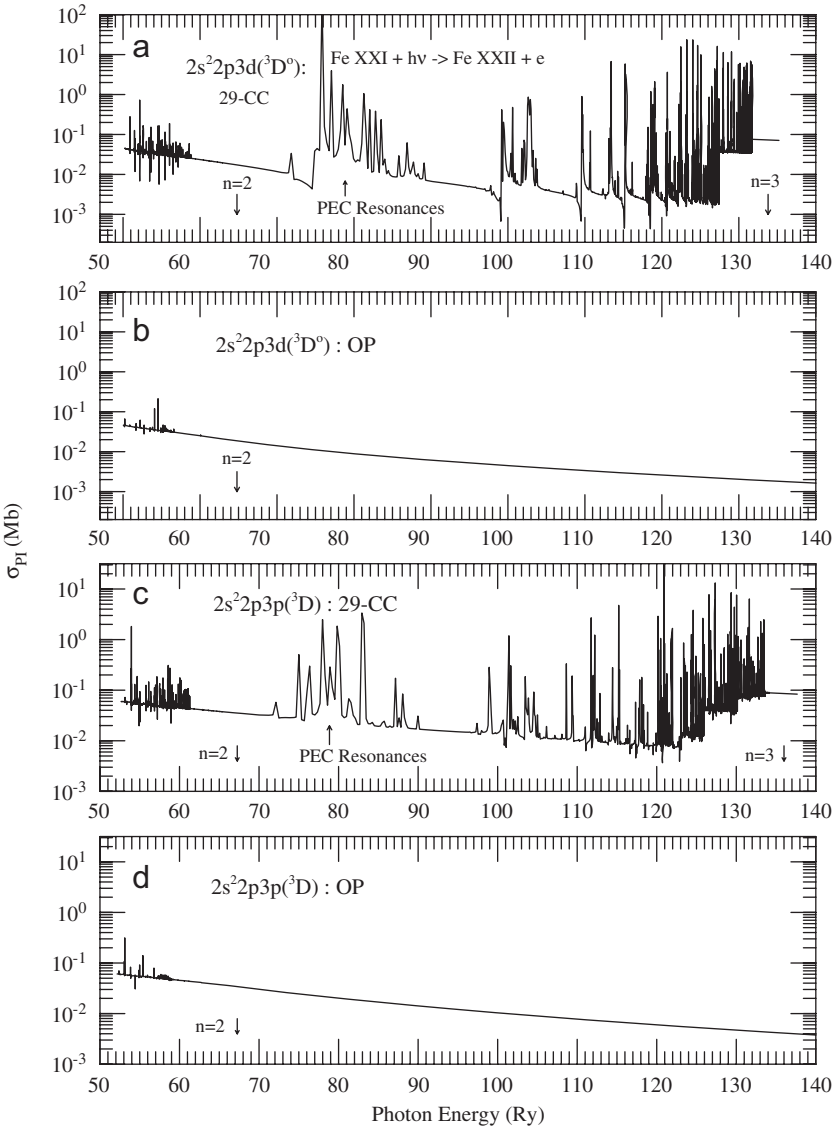

Fig. 3. Comparison of total photoionization cross section, σ_{PI}, of excited valence electron states of Fe XXI from the present work and the Opacity Project (OP) [5]: (a) present and (b) OP for the state $2s^2 2p3d(^3D^0)$; (c) present and (d) OP for the state $2s^2 2p3p(^3D)$. The present σ_{PI} shows (i) correlation effect of $n = 3$ states which introduces more enhanced resonances beyond $n = 2$ thresholds and (ii) the wide resonant structures in the energy range from about 73 to 82.5 Ry due to the PEC resonances. The $n = 2$ and 3 arrows indicate positions of the highest core states in these complexes.

magnitude. Table 1 indicates that core Fe XXII can cause eight possible PEC resonances in the energy range from about 73 Ry due to dipole allowed core excitation of $2s^2 2p(^2P^0) \rightarrow 2s^2 3s(^2S)$ to about 82 Ry for excitation $2s^2 2p(^2P^0) \rightarrow 2s2p3p(^2S)$. PEC resonances contribute considerably and introduce a 'bump' in the total recombination rates [21]. The narrow resonances up to energy corresponding to the highest target $n = 3$ threshold are Rydberg series of resonances.

Fe XXI is a highly ionized ion that exists more abundantly at high temperatures around $\sim 10^6 - 10^7$ K in plasmas [2]. Hence study of this ion in the high-energy or temperature region is highly appropriate. The computed cross section can be a factor 10 or larger than the OP cross section at high energies. This may have important effect on increased opacities in plasmas, such as, the interior opacity of the sun and hence to determination of abundances. Precise determination of solar chemical composition, from opacities or from

seismology, to explain the observation has been under considerable investigation in recent years [23,24]. Studies on other iron ions, similar to the present one, may provide the crucial key information to the investigation.

In purely photoionized plasmas Fe XXI could exist at temperatures down to 10^5 K. Fine structure couplings, especially from the quintet states that do not allow ionization below the $2s2p^2(^4P)$ core state in LS coupling, will be more important in the low energy region. Inclusion of relativistic fine structures is in the plan for future work.

As mentioned earlier, oscillator strengths and radiative decay rates for Fe XXI obtained from the bound state wavefunctions and dipole matrices are also available electronically [8]. They correspond to a total of 28,775 transitions among the 835 bound LS terms of Fe XXI.

5. Conclusion

Photoionization of $h\nu + \text{Fe XXI} \rightarrow e + \text{Fe XXII}$ is studied in detail with emphasis on the features at high energy relevant to abundance of Fe XXI in high temperatures in most astrophysical sources. Prominent resonant features due to PEC resonances of $n = 3$ core excitations in the photon energy range of 73–82 Ry are seen for the first time. Other new high-energy features have also been identified. Total and partial photoionization cross sections are presented for bound states with $n \leqslant 10$ and $l \leqslant 9$. Various features arising from coupling of channels are discussed.

The inclusion of relativistic effects in the calculations will improve the accuracy of the cross sections and rates, especially in low energy region. Coupling of channels not allowed in LS coupling, but allowed in fine structure, will introduce resonances in the low energy region and can have significant effects on low temperature photoionization and recombination rates. Study of this ion in the high-energy region for the first time in LS coupling is the most practical way since the ion has a large number of bound states requiring extensive computation.

Files for photoionization cross sections, energy levels, and oscillator strengths are available electronically from CDS and from NORAD website: www.astronomy.ohio-state.edu/nahar/nahar_radiativeatomicdata.

Acknowledgments

The author acknowledges one of the referees for pointing out the increased interior opacity of the sun by the enhanced photoionization cross sections at high energy and hence to determination of solar abundances.

This work was partially supported by the NASA Astronomy and Physics Research Analysis Program. The computational work was carried out on Cray machines at the Ohio Supercomputer Center in Columbus, OH.

References

[1] Linsky JL, Wood BE, Brown A, Osten RA. Dissecting Capella's corona: GHRS spectra of the Fe XXI 1354 and He II lambda 1640 lines from each of the capella stars. Astrophys J 1998;492:767–77.
[2] Arnaud M, Raymond J. Iron ionization and recombination rates and ionization equilibrium. Astrophys J 1992;398:394–406.
[3] Dopita MA, Sutherland RS. Astrophysics of the diffuse universe. Berlin: Springer; 2003.
[4] The Opacity Project Team. The opacity project, vol. 1, 1995, vol. 2, 1996. Institute of Physics Publishing.
[5] Luo D, Pradhan AK. Atomic data for opacity calculations. XI—the carbon isoelectronic sequence. J Phys B 1989;22:3377–95.
[6] Nahar SN, Pradhan AK. Electron-ion recombination in the close-coupling approximation. Phys Rev A 1992;45:7887–93.
[7] Zhang HL. Relativistic calculations of photoionization cross sections. Phys Rev A 1998;57:2640–50.
[8] NORAD website: ⟨www.astronomy.ohio-state.edu/nahar/nahar_radiativeatomicdata⟩.
[9] Nahar SN. Atomic data from the Iron Project XLV. Relativistic transition probabilities for carbon-like Ar XIII and Fe XXI using Breit–Paili R-matrix method. Astron Astrophys Suppl Ser 2000;127:253–70.
[10] Hummer DG, Berrington KA, Eissner W, Pradhan AK, Saraph HE, Tully JA. Atomic data from the IRON Project. 1: goals and methods. Astron Astrophys 2003;279:298–309.
[11] Burke PG, Robb WD. R-matrix theory of atomic processes. Adv At Mol Phys 1975;11:143–214.
[12] Seaton MJ. Atomic data for opacity calculations. I. General description. J Phys B 1987;20:6363–78.
[13] Berrington KA, Burke PG, Butler K, Seaton MJ, Storey PJ, Taylor KT, et al. Atomic data for opacity calculations. II. Computational methods. J Phys B 1987;20:6379–97.

[14] Berrington KA, Eissner W, Norrington PH. RMATRIX1: Belfast atomic R-matrix codes. Comput Phys Commun 1995;92:290–420.
[15] Nahar SN, Pradhan AK. Unified electron-ion recombination rate coefficients of silicon and sulfur ions. Astrophys J 1995;447:966–79.
[16] Sugar J, Corliss C. Elements: potassium through nickel. J Phys Chem Ref Data (1985); 14(Suppl. 2) listed in NIST compiled website, ⟨http://physics.nist.gov/cgi-bin/AtData/main_asd⟩.
[17] Eissner W, Jones M, Nussbaumer H. Techniques for the calculation of atomic structures and radiative data including relativistic corrections. Comput Phys Commun 1974;8:270–306.
[18] Nahar SN, Pradhan AK. Unified treatment of electron–ion recombination in the close-coupling approximation. Phys Rev A 1994;49:1816–35.
[19] Nahar SN. Total electron–ion recombination of Fe iii. Phys Rev A 1996;53:2417–24.
[20] Nahar SN. Atomic data from the Iron Project LXI. Radiative E1, E2, E3, and M1 transition probabilities for Fe IV. Astron Astrophys 2006;448:779–85.
[21] Nahar SN. Photoionization and electron–ion recombination of Fe XXI. 2008, in preparation.
[22] Yu Y, Seaton MJ. Atomic data for opacity calculations. IV. Photoionisation cross sections for C II. J Phys B 1987;20:6409–29.
[23] Asplund M, Grevesse N, Sauval J. The solar chemical composition. arXiv 2004;astro-ph/0410214v2.
[24] Delahaye F, Pinsonneault MH. The solar heavy-element abundances. I. Constraints from Stellar Interior. Astrophys J 2006;649:529–40.